PAPER

# Tailoring terahertz radiation by controlling tunnel photoionization events in gases

New Journal of Physics
The open-access journal for physics

# Tailoring terahertz radiation by controlling tunnel photoionization events in gases

**I Babushkin[1,6], S Skupin[2,3], A Husakou[4], C Köhler[2], E Cabrera-Granado[2], L Bergé[5] and J Herrmann[4]**

[1] Weierstraß-Institut für Angewandte Analysis und Stochastik, 10117 Berlin, Germany
[2] Max Planck Institute for the Physics of Complex Systems, 01187 Dresden, Germany
[3] Friedrich Schiller University, Institute of Condensed Matter Theory and Optics, 07743 Jena, Germany
[4] Max-Born-Institut für Nichtlineare Optik und Kurzzeitspektroskopie, 12489 Berlin, Germany
[5] CEA-DAM, DIF, F-91297 Arpajon, France
E-mail: babushkin@wias-berlin.de

*New Journal of Physics* **13** (2011) 123029 (16pp)
Received 28 August 2011
Published 21 December 2011
Online at http://www.njp.org/
doi:10.1088/1367-2630/13/12/123029

**Abstract.** Various applications ranging from nonlinear terahertz (THz) spectroscopy to remote sensing require broadband and intense THz radiation, which can be generated by focusing two-color laser pulses into a gas. In this setup, THz radiation originates from the buildup of electron density in sharp steps of attosecond duration due to tunnel ionization, and the subsequent acceleration of free electrons in the laser field. We show that the spectral shape of the THz pulses generated by this mechanism is determined by the superposition of contributions from individual ionization events. This provides a straightforward analogy to linear diffraction theory, where the ionization events play the role of slits in a grating. This analogy offers simple explanations for recent experimental observations and opens new avenues for THz pulse shaping based on temporal control of the ionization events. We illustrate this novel technique by tailoring the spectral width and position of the resulting radiation using multi-color pump pulses.

[6] Author to whom any correspondence should be addressed.

## Contents



## 1. Introduction

In recent years, terahertz (THz) technology has attracted much attention, because it can provide unique analytical and imaging tools for nonlinear and time-domain spectroscopy, remote sensing, biology and medicine, security screening and information and communication technology (see e.g. [1–4]). Among the various THz sources, employing two-color ionizing femtosecond pulses in gases [5, 14] stands out because of absence of damage threshold, low phonon absorption and zero interface reflection. The two-color scheme provides striking performance in terms of bandwidth that can exceed 100 THz and thus even covers far- and mid-infrared, as well as high peak fields up to the MV $cm^{-1}$ range.

In the standard realization of this method, a femtosecond laser pulse and its second harmonic (SH) are collinearly focused into a gas, such as ambient air, yielding powerful THz radiation with well-defined electric field values. Initially, this process was explained by four-wave mixing rectification via third-order nonlinearity [5, 12]. However, a threshold for THz generation [6, 10] as well as plasma current measurements [13] indicated that plasma formation plays an important role in the generation process. In addition, the Kerr nonlinearity is far too small [7, 15] to explain the observed THz field strength in such a setup. In order to solve this discrepancy, Kim *et al* [11, 13] have put forward the so-called photocurrent mechanism. In this mechanism, tunneling ionization and subsequent electron motion produce a quasi-dc photoinduced current, which in turn emits THz radiation. The quasi-dc plasma current can be efficiently produced in a gas irradiated with two-color laser pulses [5–14], in multicolor pump schemes [16] and in chirped [17] or few-cycle pulses [18, 19]. There are other, generally less efficient mechanisms for THz generation in gases that employ single-color pumps. Such mechanisms involve ponderomotive effects in a preformed plasma [20], excitation of plasma oscillations [21–23] or conical Cherenkov radiation [24–26].

The results published so far [10, 13, 15, 16, 27–31] provide several important features of the THz spectrum. However, a general framework for the analysis, control and design of THz radiation is still missing. Similar to pulse-shaping techniques in the optical range, the broadband control of THz waveforms and its spectral properties is highly desirable for many applications, while the existing techniques are applicable only to a narrow bandwidth of a few THz [30, 32, 33].

In this paper, we advance the understanding of the fundamental physics of THz generation in gases as well as examine the basic mechanism associated with plasma formation. We demonstrate that THz generation in gases is intrinsically connected to the optically induced stepwise increase of the plasma density due to tunneling ionization. New spectral components are emitted in a discrete set of attosecond-scale, ultra-broadband bursts associated with these ionization events; in the spectral representation, THz emission results from an interference of these radiation bursts.

Using appropriate field shapes of the pump pulses, e.g. tuning the frequencies and phases of two- or multi-color pulses, the temporal positions of the ionization events can be controlled. In turn, this allows us to design the emitted radiation within a broad spectral range of more than 100 THz. This new concept of prescribing the phase and amplitude of each elementary contribution responsible for THz emission has a remarkable analogy in linear diffraction theory: the produced spectrum can be understood like the far-field diffraction pattern of a grating, where the ionization events play the role of slits. A comprehensive (3 + 1)-dimensional non-envelope model of propagation is used to verify by means of numerical simulations that the simple picture drawn above captures the essential physics of THz generation.

## 2. Structure of the THz spectrum

We start our analysis in the so-called local current (LC) limit; that is, we consider a small volume of gas irradiated with the strong pump field $E(t)$ (see figure 1(a)). Electrons produced due to ionization build up a current $J(t)$, which, in turn, produces an electromagnetic wave $E^J(t) \propto \partial_t J(t)$ [34]. We focus here on the pump intensities where tunnel ionization is the dominant ionization process. In this regime, the free electron density $\rho(t)$ increases stepwise in short attosecond-scale ionization events corresponding to maximum amplitudes of the pump field at times $t_n$ (see figure 1(c)). This stepwise increase of the free electron density $\rho(t)$ was recently confirmed experimentally [35, 36]. The ionization events are well separated from each other and thus $\rho(t)$ can be written as a sum over contributions from all ionization events: $\rho(t) = \sum_n \delta\rho_n H_n(t)$. Each ionization event has a well-defined amplitude $\delta\rho_n$ and shape $H_n(t)$. In the following, we assume that all ionization events yield analogous plasma steps $H_n(t) \simeq H(t - t_n)$, where $H$ is a 'smoothed' step function (see the green filled curve in figure 1(c)). An approximate analytical formula for $H(t)$ is given in appendix A.1. We note that the actual form of the steps may deviate from the predictions of the quasi-static formula for tunneling ionization (see e.g. [35, 37–39]). Nevertheless, the step-wise character of ionization events remains valid for a Keldysh parameter around unity [36, 39], which corresponds to the intensities considered here. Only this step-wise character of the ionization events will be important in the following analysis.

In figures 1(b)–(e) an exemplary two-color pump field $E(t) = \mathcal{E}(t)[\cos(\omega_0 t) + r\cos(2\omega_0 t + \theta)]$ is considered, where $\omega_0 = 2\pi \times 375\,\mathrm{ps}^{-1}$ is the fundamental frequency (corresponding to the wavelength of 800 nm), $r = \sqrt{0.2}$ and $\theta = \pi/2$ are the relative amplitude and phase of the SH component. For such a two-color pulse (and assuming $r < 1$) the positions of ionization events are given by $\omega_0 t_n \approx \pi n - 2(-1)^n r \sin\theta$ [15]. $\mathcal{E}(t)$ is a Gaussian pulse envelope shape with full-width at half-maximum (FWHM) pulse duration $\tau_{\mathrm{in}} = 40\,\mathrm{fs}$, with a peak intensity of $100\,\mathrm{TW\,cm}^{-2}$ for the fundamental component.

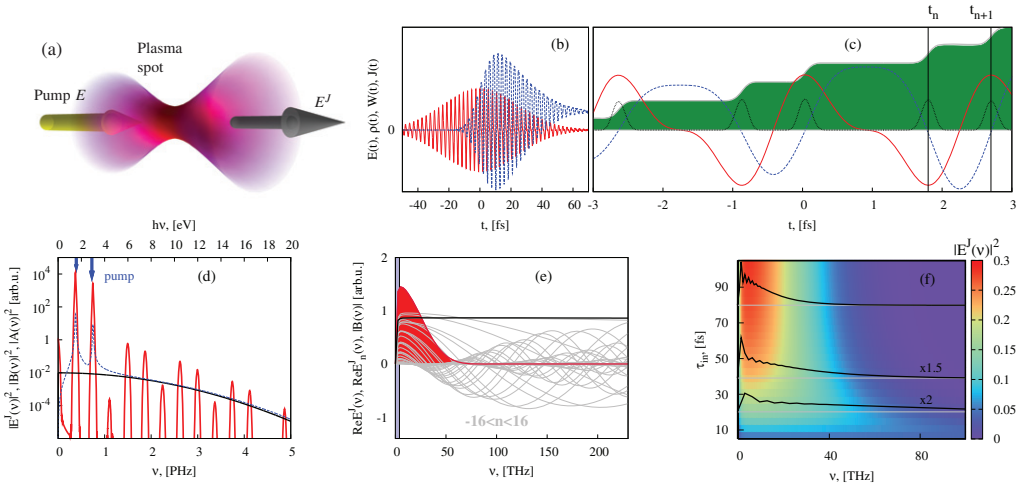


**Figure 1.** Mechanism and spectral properties of terahertz generation by ionizing two-color pulses. (a) Schematic setup; (b) two-color pump field $E(t)$ (red curve) and current $J(t)$ (dashed blue curve) induced by tunneling ionization; (c) stepwise modulation of the free electron density (filled green curve) and ionization rate $W(t)$ (thin dotted black curve); besides, a few cycles of the electric field $E(t)$ (red curve) and the current $J(t)$ (dashed blue curve) are shown. (d) Spectrum $|E^J(\nu)|^2$ versus frequency $\nu = \omega/2\pi$ on a large frequency scale (red curve). Each ionization event at time $t_n$ induces broadband radiation described by the form-factors $B(\nu)$ (black curve) and $A_n(\nu)$ (dashed blue curve). The sum of all partial contributions in equation (2) yields the resulting spectrum $E^J(\nu)$. (e) Partial contributions Re $E^J_n(\nu)$ from the $n$th ionization event for $-16 < n < 16$ (gray curves) and the total spectrum Re $E^J(\nu)$ (filled red curve) in the THz-to-mid-infrared spectral region (Im $E^J(\nu)$ is negligible here). The black curve shows $B(\nu)$. The decay of $E^J(\nu)$ for $\nu \gtrsim 20\,\mathrm{THz}$ is solely due to destructive interference of different $E^J_n(\nu)$. In contrast, in the shaded region ($\nu < 5\,\mathrm{THz}$) $E^J(\nu)$ decays because of a decrease of $B(\nu)$. (f) Spectrum $|E^J(\nu)|^2$ versus input pulse duration $\tau_{\mathrm{in}}$ for a fixed peak intensity. As the number of ionization events decreases with $\tau_{\mathrm{in}}$, the spectral width increases, as also confirmed by three-dimensional (3D) simulations for $\tau_{\mathrm{in}} = 20$, 40 and 80 fs (black curves).

With the assumption that electrons are born with zero initial velocity, the plasma current $J(t)$ (blue curves in figures 1(b) and (c)) is governed by

$$\partial_t J(t) + \gamma J(t) = \frac{q^2}{m} E(t)\rho(t), \tag{1}$$

where $\gamma$ is the phenomenological electron–ion collision rate ($\gamma \cong 5\,\mathrm{ps}^{-1}$ at atmospheric pressure) and $m$ and $q$ are electron mass and charge [15, 23, 40]. In equation (1), ponderomotive forces are neglected because they play only a minor role in the situation considered here [15, 20].

Then, in the Fourier domain the generated electromagnetic wave in the LC limit $E^J(\omega) \propto \omega J(\omega)$ reads (see appendix A.1)

$$E^J(\omega) = \sum_n [A_n(\omega) - C_n B(\omega)]\, \mathrm{e}^{\mathrm{i}\omega t_n}. \tag{2}$$

Here, $A_n(\omega) = -\mathrm{i}qg\omega\delta\rho_n\mathcal{F}[H(t)v_\mathrm{f}(t+t_n)]$, $C_n = q\delta\rho_n v_f(t_n)$ and $B(\omega) = -\mathrm{i}g\omega\mathcal{F}[H(t)\mathrm{e}^{-\gamma t}]$, with $\mathcal{F}$ denoting the Fourier transform, $v_\mathrm{f}(t) = \frac{q}{m}\int_{-\infty}^{t} E(\tau)\,\mathrm{e}^{\gamma(\tau-t)}\mathrm{d}\tau$ is the free electron velocity, and $g$ is a constant.

Equation (2) allows us to identify the impact of each ionization event. The interpretation of equation (2) is straightforward when we consider the spectral dependence of the amplitudes $A_n(\omega)$ and $B(\omega)$, which can be calculated analytically in a reasonable approximation (see appendix A.1):

$$B(\omega) \propto \frac{\omega}{\omega - \mathrm{i}\gamma}\exp\left(-\frac{\omega^2}{\sigma^2}\right), \tag{3}$$

where $\sigma \cong 10\,\mathrm{fs}^{-1}$ is the spectral width of a typical ionization peak (see thin black curves in figure 1(c)). In contrast to $B(\omega)$, the amplitudes $A_n(\omega)$ depend nontrivially on the pump pulse. Examples of $A_n(\omega)$ and $B(\omega)$ are shown in figures 1(d) and (e). $B(\omega)$ features two clearly separated frequency scales determined by $\gamma$ and $\sigma$. On the short frequency scale $\omega \lesssim \gamma$ (up to 5 meV or ~0–2 THz for atmospheric pressure), $B(\omega) \propto \omega$, whereas for larger frequencies, $B(\omega)$ depends only slowly on $\omega$ (on the scale of ~10 eV). We note that, for frequencies above several eV, the real spectral shape may become more complicated due to the influence of higher order effects [35, 37, 41, 42].

If we consider the range from a few to approximately 100 THz, equation (2) can be significantly simplified. In this range, $B(\omega)$ can be considered as a constant, and additionally the $A_n(\omega)$ are negligible as seen from figure 1(d), so that

$$E^J(\omega) = B(\omega)\sum_n C_n\,\mathrm{e}^{\mathrm{i}\,\omega t_n} \propto \sum_n C_n\,\mathrm{e}^{\mathrm{i}\,\omega t_n}. \tag{4}$$

In other words, the resulting THz spectrum is a simple linear superposition of the contributions $E_n^J = C_n\,\mathrm{e}^{\mathrm{i}\,\omega t_n}$ and its structure is mainly governed by interference due to the spectral phases $\mathrm{e}^{\mathrm{i}\,\omega t_n}$. This interference is illustrated in figure 1(e) (cf also figure 2(b)). Note that in the temporal domain, equation (4) corresponds to a set of sharp peaks localized near $t_n$, each of them having the amplitude $C_n$ and the shape $\partial_t[H(t-t_n)\mathrm{e}^{-\gamma(t-t_n)}]$. Thus, equation (4) describes sharp attosecond-long bursts of radiation localized near the ionization events.

Further, the same simple superposition principle is valid also for higher frequencies in the more general equation (2). Indeed, figure 1(d) shows that constructive spectral interference in equation (2) appears also for frequencies $\omega \sim l\omega_0$, where $l$ is an integer. This finding is consistent with recent experimental results [36], where optical harmonics generated due to tunneling-ionization-induced modulations of the electron density were observed. Therefore, our superposition principle may also offer a complementary understanding of Brunel radiation [36, 43].

In fact, equation (4) shows that THz generation can be understood completely analogous to far-field interference patterns produced by a diffraction grating [44], where the ionization events play the role of slits. Each such 'slit' produces a broad 'secondary wave', and their interference results in narrow lines, according to the Huygens–Fresnel principle [44]. THz radiation then corresponds to the zeroth diffraction order. In contrast to diffractive gratings, interference here takes place in the frequency domain and not in position space.

In a somewhat oversimplified picture, one can explain the spectrum shown in figure 1(d) analogous to interference patterns produced by diffraction gratings of equidistant slits,

$$E^J(\omega) \sim \sin(N\omega\delta t/2)/\sin(\omega\delta t), \tag{5}$$

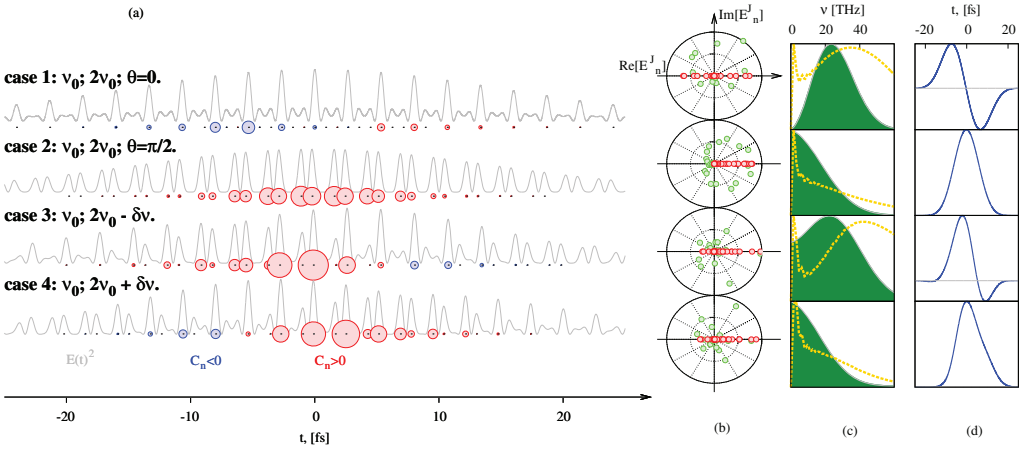


**Figure 2.** Interference of contributions from different ionization events (a, b), THz spectrum (c) and temporal shape (d) for different values of the phase $\theta$ between the fundamental and SH (cases 1, 2) as well as of the frequency shift $\pm\delta\nu$ of the SH (cases 3, 4; $\delta\nu = 20$ THz, $\theta = \pi/4$). (a) Times of ionization events $t_n$ (center of circles) and amplitudes $C_n$ (radii of circles; red (blue) color indicates positive (negative) sign). The gray curves show the electric field amplitude $E^2(t)$ of the pump pulse. (b) Values of the summands in equation (4) $E_n^J(\nu)$ in the complex plane for $\nu \cong 0$ (red circles) and $\nu = 25$ THz (green circles). For cases 1 and 3, destructive interference occurs at $\nu \cong 0$ and is partially compensated at larger frequencies. (c, d) Corresponding THz spectral shapes and temporal profiles obtained from equation (4) ($\sum_n E_n^J$, filled green curve) and from 3D simulations at the linear focus $z = 5$ mm (dashed yellow curves). Note that the amplitudes for case 1 are about one order of magnitude smaller in comparison to the other cases.

where $N$ is the number of ionization events and $\delta t \sim \pi/\omega_0$ is the time interval between two subsequent ionization events (see appendix B). The width of the spectral line is inversely proportional to $N$, i.e. to the input pulse duration (see figure 1(f)). Such an inverse dependence of the THz spectral width on the pump duration has already been observed experimentally [7]. It is also compatible (black lines in figure 1(f)) with comprehensive 3D simulations, where propagation and transverse effects are accounted for (see appendix A.2).

## 3. Control of the THz spectrum

Understanding the spectrum of the radiation emitted by the plasma current $J$ as an interference pattern provides deeper insight into the mechanism responsible for the THz generation. Beyond that, this understanding provides us with the possibility of shaping the emitted radiation by suitably engineering the pump field. Here, we will restrict ourselves to the THz and far-infrared domain described by equation (4). The latter indicates that, in order to control the THz spectral shape, we have to target the times of the ionization events $t_n$ and the values of $C_n = q\delta\rho_n v_f(t_n)$.

Figure 2 shows several examples of THz generation from simple variations of the two-color scheme. The variations of the relative phase $\theta$ between fundamental and SH components of the pump pulse have a strong influence on the THz spectral shape (see cases 1 and 2), in

addition to the known dependence of the THz yield [13, 45]. This observation can be readily explained within our linear interference framework. For $\theta \cong 0$ (case 1) the coefficients $C_n$ are not sign definite (red and blue circles in figure 2(a)). Thus, for $\omega \cong 0$, different contributions in equation (4) cancel each other; that is, destructive interference dominates. Nevertheless, with increasing frequency $\omega$ the destructive interference is (partially) compensated for by the spectral phases $e^{i\omega t_n}$. This behavior is shown in figure 2(b), where contributions from the ionization events $E_n^J$ are visualized in the complex plane for different frequencies $\omega$. Consequently, the spectral maximum is shifted from zero (see figure 2(c)). In contrast, for $\theta = \pi/2$ (case 2) all coefficients $C_n$ are positive. This obviously ensures that at $\omega \cong 0$ constructive interference dominates, and the phase factor $e^{i\omega t_n}$ can lead only to destructive interference when $\omega$ is increased. Therefore, the spectral maximum is located at zero frequency in this case. Moreover, the coefficients $C_n$ are much larger in amplitude, which explains the increased THz yield for $\theta = \pi/2$.

We verified this behavior by comprehensive (3 + 1)-dimensional (3D) numerical modeling (see appendix A.2), which was recently successfully compared to experiments [15]. We consider a Gaussian input beam with width $w_0 = 100\,\mu$m and duration (FWHM) $\tau_{in} = 40$ fs for the 800 nm fundamental pump pulse (pulse energy $\sim$300 μJ). The energy of the SH at 400 nm is chosen as 7.5% of the fundamental, with duration and width smaller than the values for the fundamental by a factor $\sqrt{2}$ (similar to typical experimental conditions). These pulsed input beams are focused with $f = 5$ mm into argon at atmospheric pressure. In contrast to the simple LC model, the phase angle $\theta$ between the two components shifts during propagation. For our particular configuration, an initial value $\theta_{in} \cong \pi/4$ guarantees maximum THz energy yield of $\sim 1.8\,\mu$J; $\theta_{in} \cong -\pi/4$ leads to a minimum yield of $0.25\,\mu$J; the generic value $\theta_{in} = 0$ yields $\sim 1\,\mu$J. THz spectra obtained for the two extremal cases are shown in figure 2(c), cases 2 and 1, respectively (dashed yellow curves). They agree remarkably well with the predictions obtained from equation (4), where the extremal cases correspond to $\theta = 0$ and $\theta = \pi/2$ due to absence of propagation effects.

We also observe a high sensitivity of the THz spectra towards detuning of the relative frequency ratio between the two pump components (see cases 3 and 4 in figure 2). Such pulses with the so-called incommensurate SH (frequency $2\nu_0$ is shifted by $\delta\nu$) offer straightforward control of the position of the maximum THz spectral intensity, without decreasing the total THz yield. Recently, this shift of the THz spectrum with $\delta\nu$ was predicted [27] and demonstrated experimentally [28]. Again, we can use our linear interference framework to explain this effect. The responsible shifts of the ionization events can be computed approximatively (see appendix B) as $\omega_0 t_n \approx n\pi - 2r(-1)^n \sin(\theta \pm \pi n \delta\nu/\nu_0)$. The SH frequency shift $\pm\delta\nu$ makes the effective phase angle $n$ dependent and thus shifts the ionization events in time. Using our diffraction-grating analogy, the effect corresponds to increasing or decreasing the slit distance along the grating. This frequency shift can also be calculated analytically under some further approximations (see appendix B).

Because the coefficients $C_n$ are not sign definite (see figures 2(a) and (b), the 'secondary waves' are not in-phase), such a non-equidistant grating can lead to a spatial shift of the zeroth diffraction order, i.e. a frequency shift of the maximum THz spectral intensity. As is seen from figures 2(c) and 3(a), the THz frequency shift is not symmetric with respect to the sign of $\delta\nu$. This effect occurs for pulses with finite duration (see also appendix B).

Again, our predictions from equation (4) are in good agreement with 3D numerical simulations. Incommensurate two-color pulses clearly produce the predicted THz spectral shift

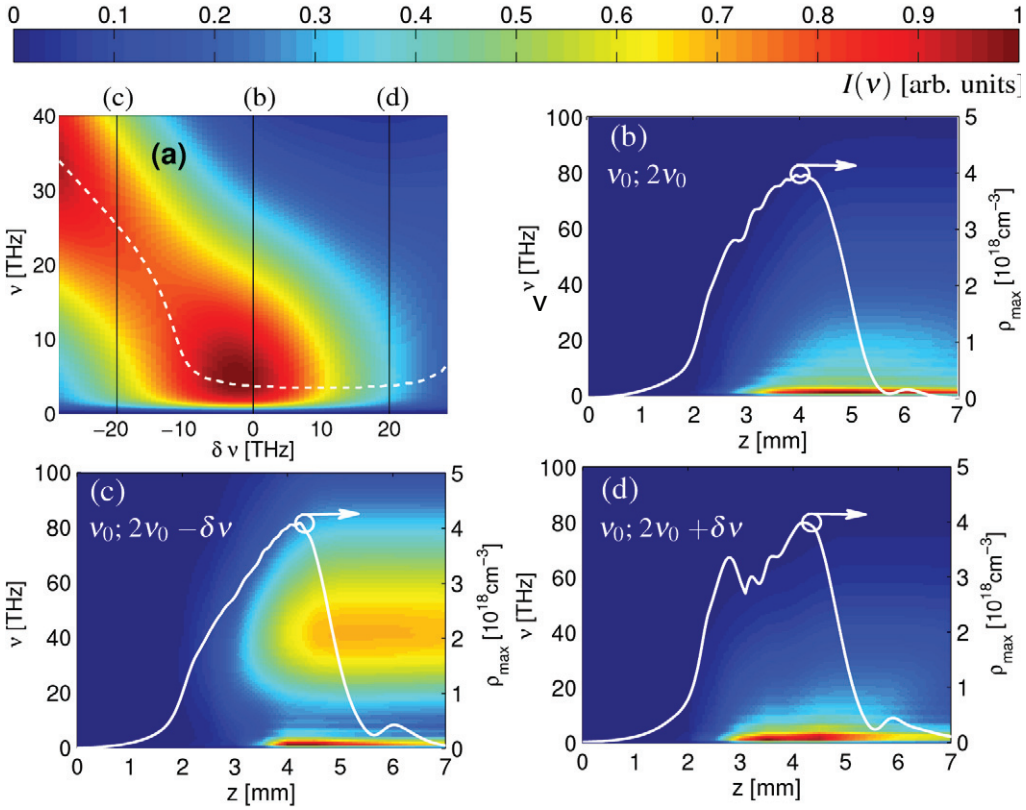


**Figure 3.** THz generation by two-color pump pulses with incommensurate frequencies. (a) THz spectrum versus frequency shift $\delta\nu$ of the SH computed from equation (2). The dashed white line shows the position of the spectral maximum. (b–d) THz spectrum (color plot) as well as the maximum plasma density (white line) along the propagation axis according to 3D simulations for frequency shifts equal to 0 and $\pm 20$ THz, respectively.

for negative SH detuning (see figure 3). Neither linear nor nonlinear propagation effects due to focusing or laser-induced plasma seem to jeopardize this effect. The energy in the shifted THz pulse is $\sim 1\ \mu$J, as in the corresponding commensurate case (see figure 3(b)). On the other hand, figure 3(d) reveals that, as expected, a positive SH detuning does not alter the THz spectral shape significantly, but the energy yield decreases by a factor of two to $\sim 0.5\ \mu$J. We note that, according to [46], the THz radiation is emitted predominantly from the plasma surface. For figure 3 this means that, for smaller values of $z$, the THz radiation is emitted at earlier time instants before the plasma reaches its maximum density.

Let us, finally, consider a more complex example of THz spectral engineering. Namely, we attempt to significantly increase the spectral width by using a field shape which optimizes the 'amplitudes' $C_n$ of just a few ionization events, suppressing the others. This leads to THz-to-mid-infrared supercontinuum, which is of great importance for many applications. For this purpose, we resort to a three-color pump setup involving an optical parametric amplifier (OPA) [47]. We assume a fundamental frequency $\nu_0 = 375$ THz ($\lambda_0 = 800$ nm) and signal and idler frequencies $\nu_\mathrm{s}$ and $\nu_\mathrm{i}$ obeying $\nu_\mathrm{s} + \nu_i = \nu_0$ ($\nu_\mathrm{s} = 0.55\nu_0$, $\nu_\mathrm{i} = 0.45\nu_0$). From figure 4(b), one can see that in such a configuration only a few ionization events have large amplitudes $|C_n|$. This immediately leads to a much broader THz spectrum, as is obvious from the

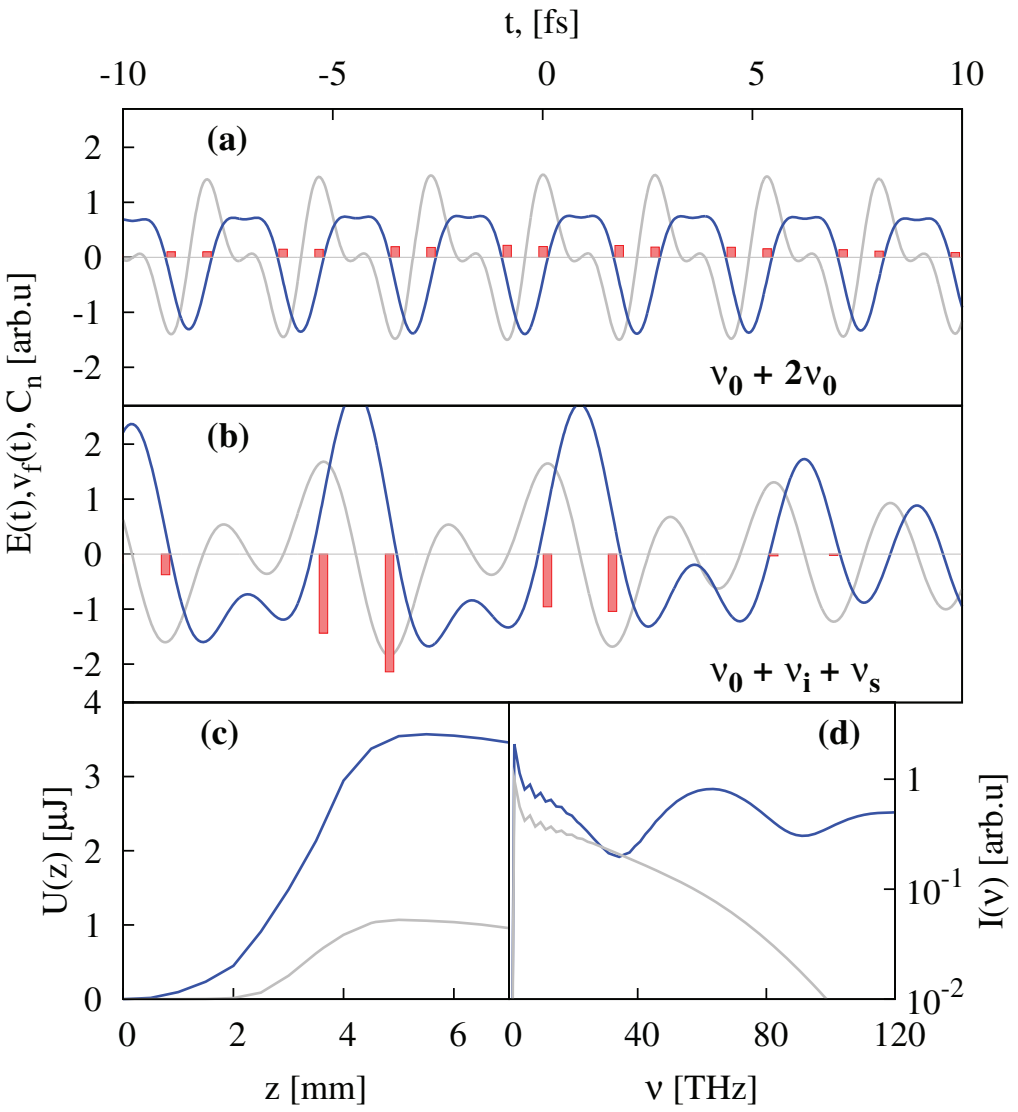


**Figure 4.** Comparison of the THz characteristics produced by two- and three-color pump pulses. (a) Field shape $E(t)$ (gray line), free electron velocity $v_f(t)$ (blue line) as well as ionization amplitudes $C_n$ (bars at ionization events) for the two-color pump (see figure 1). (b) The same quantities for the three-color pump, e.g. for an OPA with frequencies $\nu_0 = \nu_s + \nu_i$ ($\nu_s = 0.55\nu_0$, $\nu_i = 0.45\nu_0$). (c) THz energies $U$ versus propagation distance $z$ according to 3D simulations and (d) corresponding spatially integrated THz spectra at the position of the linear focus $z = 5$ mm for the three-color (blue lines) and two-color (gray lines) cases.

above-discussed diffraction grating analogy. In figures 4(c) and (d), the results of 3D simulations for this case are shown, assuming that each of the three pump components contains one-third of the total pulse energy of 300 $\mu$J, while all other parameters are kept unchanged.

Quite interestingly, the three-color configuration we use provides much larger values for the $|C_n|$ than the previous two-color scheme with comparable pump energy (cf figures 4(a) and

(b)). In the LC limit, the resulting THz yield is about 40 times larger. In our simulations, this increased THz yield is indeed visible in the beginning of the propagation $z < 2.5$ mm. However, upon further propagation, saturation effects, mainly coming from plasma defocusing of the pump and depletion of neutral atoms, limit the total THz energy to a few $\mu$J.

## 4. Conclusion and outlook

In summary, we have shown that THz emission in gases by multi-color laser fields is intrinsically connected with the attosecond jumps of the plasma density induced by tunneling ionization. The THz spectrum is described by a superposition of the spectrally ultrabroad contributions from separate ionization events.

This approach explains the basic features of THz radiation such as the inverse dependence of the spectral width on the pulse duration and the shift of THz spectral maxima for non-integer frequency offsets of two-color pumps. Thus, although our simple picture does not include several secondary effects, such as the influence of plasma oscillations, ponderomotive forces, exact shape of ionization steps and others, it provides an easy prediction of the THz spectrum for arbitrary input field shapes. This insight opens the possibility of manipulating the THz waveform and of shaping the THz spectrum by controlling the tunneling photo-ionization. In the present paper, we demonstrated only basic features of such a control, using frequencies and phases of two- or three-color pump fields. We note that other degrees of freedom of light such as polarization or spatial shape of the pump pulses can also be used for THz control. Noteworthy, our approach is not limited to the THz, far- and mid-infrared range but can be potentially extended to frequencies much higher than the pump one, i.e. to optical harmonics.

We believe that this novel strategy for controlling fundamental properties of THz pulses could become a basic tool in optical technology: an ultra-broadband pulse shaper working in the range from THz to mid-infrared. Just as optical pulse shapers for femtosecond pulses are indispensable in ultrafast physics, the proposed THz control can find promising applications in many fields of research, including, among others, THz time-domain spectroscopy, chemical reaction dynamics and optical signal processing.

## Acknowledgments

This work was performed using high-performance computing resources at Rechenzentrum Garching and from the Grand Equipement National pour le Calcul Intensif–Centre de Calcul pour la Recherche et la Technologie (GENCI-CCRT) (grant no. 2011-106003). IB acknowledges support from the Deutsche Forschungsgemeinschaft (DFG; grant no. 4156/1-1) and EC-G acknowledges support from project no. FIS2009-07870 (Ministerio de Ciencia y Tecnologia).

## Appendix A. Mathematical modeling

### *A.1. Discrete ionization model*

The electron density $\rho(t)$ is described by the equation

$$\partial_t \rho = W_{\mathrm{ST}}(E)[\rho_{at} - \rho(t)], \tag{A.1}$$

where $\rho_{at}$ denotes the neutral atomic density. We use a quasi-static tunneling ionization rate for hydrogen-like atoms [10, 15]:

$$W_{ST}(E) = 4\omega_a (r_H)^{2.5} [E_a/|E|] \exp[-2(r_H)^{1.5} E_a/3|E|], \tag{A.2}$$

where $E_a = m^2 q^5/(4\pi\varepsilon_0)^3\hbar^4$, $\omega_a = mq^4/(4\pi\varepsilon_0)^2\hbar^3$ and $r_H = U_{Ar}/U_h$. $U_h$ and $U_{Ar}$ are the ionization potentials of hydrogen and argon, respectively. In our simulations, we employ intensities of the fundamental frequency of about 100 TW cm$^{-2}$, which correspond to a Keldysh parameter $\gamma_K \approx 1$. In this intensity range, the step-wise character of the ionization yield has already been demonstrated experimentally [35, 36].

Supposing that the ionization process occurs only near extrema of the pump electric field at times $t_n$, one finds that $E(t) \approx E_0 + E_2(t-t_n)^2$ with $E_2 = \partial_{tt} E(t_n)/2$ and $E_0 = E(t_n)$. Then, assuming $\rho_{at} \gg \rho$, we can evaluate $W_{ST}(E) \approx W_{ST}[E(t_n)] \exp\{-\sigma^2(t-t_n)^2/4\}$, where $\sigma^2 = 8(r_H)^{1.5} E_a |E_2|/3|E_0|^2$, and find that

$$\rho(t) = \sum_n \delta\rho_n H(t-t_n), \tag{A.3}$$

with

$$H(t-t_n) \propto \int_{-\infty}^{t} e^{-\frac{\sigma^2(\tau-t_n)^2}{4}} d\tau = \sqrt{\frac{\pi}{\sigma^2}} \left\{1 + \mathrm{erf}\left[\frac{\sigma(t-t_n)}{2}\right]\right\},$$

where $\mathrm{erf}(x)$ denotes the usual error function. Strictly speaking, $\sigma$ is different for every ionization event. The difference, however, is typically less than a few per cent, so we assume here a 'typical' value $\sigma \cong 10\,\mathrm{fs}^{-1}$.

The free electron current $J$ is given by

$$J(t) = q \int_{-\infty}^{t} [\partial_\tau \rho(\tau)]\,[v_f(t) - e^{\gamma(\tau-t)} v_f(\tau)]\, d\tau,$$

which is equivalent to equation (1) (see [11, 15, 29]). Using equation (A.3), $J$ can be written as a sum over all contributions from separate ionization events $J(t) = \sum_n J_n(t)$, and hence

$$J(t) = \sum_n q\delta\rho_n H(t-t_n)\{v_f(t) - e^{\gamma(t_n-t)} v_f(t_n)\}. \tag{A.4}$$

In the LC limit, assuming that the plasma source is contained in a small volume $\Delta V$, the field produced by the plasma current $J(\omega)$ in the frequency domain is $E^J = g\omega J(\omega)$ [34], where $g = i\frac{\omega\Delta V}{4\pi\varepsilon_0 c^2 r}\exp(i\omega\frac{r}{c})$, $c$ is the speed of light, $\varepsilon_0$ is the vacuum permittivity and $r$ is the distance between the plasma source and the point where the field is measured.

Thus, in order to obtain equation (2), we have to multiply the Fourier transform of equation (A.4) by $-i\omega g$. Further on, by performing the Fourier transform of $H(t)\exp(-\gamma t)$ and neglecting a slowly varying phase term $\exp(-2i\gamma\omega/\sigma^2)$, we obtain equation (3).

### *A.2. Comprehensive numerical model*

We use the unidirectional pulse propagation equation [15, 48] for linearly polarized pulses

$$\partial_z E(\omega) = i\sqrt{k^2(\omega) - k_x^2 - k_y^2}\, E(\omega) + i\frac{\mu_0\omega^2}{2k(\omega)}\mathcal{P}_{NL}(\omega). \tag{A.5}$$

Here, $E(k_x, k_y, z, \omega)$ is the relevant electric field component in the Fourier domain with respect to the transverse coordinates $(x, y)$ and time, $k = \omega n(\omega)/c$ is the wavenumber, $c$ is the speed

of light and $n(\omega)$ is the linear refractive index of argon [49]. The nonlinear polarization $\mathcal{P}_{\rm NL}(\omega) = P_{\rm Kerr}(\omega) + {\rm i}J(\omega)/\omega + {\rm i}J_{\rm loss}(\omega)/\omega$ accounts for third-order nonlinear polarization $P_{\rm Kerr}(t)$, electron current $J(t)$ and a loss term $J_{\rm loss}(t)$ due to photon absorption during ionization. The plasma current $J(t)$ is described by equation (1). The phenomenological decay constant $\gamma$ describes losses due to electron–ion collisions. Among others, this constant leads to strong absorption in the low frequency range.

In our 3D numerical code, equations (1), (A.5) and (A.1) are solved using a standard spectral operator splitting scheme. Particular attention is paid to resolve all relevant time scales, from tens of attoseconds (ionization steps) to a few picoseconds (THz radiation).

Although, strictly speaking, equation (A.5) does not describe the propagation of waves below the plasma frequency properly, this plays only a minor role because the THz radiation is emitted from the leading plasma front and thus does not propagate in the plasma [46]. Despite the fact that equations (1), (A.1), (A.5) and (A.3) neglect many further effects linked to plasma oscillations [19], ponderomotive forces [20] or the exact shape of ionization steps [37, 41], spectra obtained using equation (A.5) were found to be in good agreement with experimental results [15].

## Appendix B. Analytical description of THz emission from a two-color square-shaped pulse

We consider for simplicity the case of a two-color pulse with duration $T_0$ having the square-shaped envelope $E(t) = 0$ for $|t| > T_0/2$ and

$$E(t) = A_1 \cos\{\omega_0 t\} + A_2 \cos\{(2\omega_0 + \delta\omega)t + \theta\} \tag{B.1}$$

for $|t| \leqslant T_0/2$. Here $\delta\omega$ is a detuning from the SH, which is assumed to be small compared to the main frequency ($\delta\omega \ll \omega_0$). We also neglect the plasma decay $\gamma$ and assume $r \equiv A_2/A_1 \ll 1$.

To determine the positions $t_n$ of the tunneling ionization events (maxima of the electric field) along the time axis we equate the time derivative of equation (B.1) to zero, set $t_n = t_{n0} + \delta t_n$ and expand the resulting expression up to first orders in $\delta\omega$ and $\delta t_n$, yielding

$$\begin{aligned}\omega_0 t_n &\approx n\pi - 2r(-1)^n \left( n\pi \frac{\delta\omega}{\omega_0} \cos\theta + \sin\theta \right) \\ &\approx n\pi - 2r(-1)^n \sin\left( \theta + n\pi \frac{\delta\omega}{\omega_0} \right),\end{aligned} \tag{B.2}$$

where it is assumed that $\pi n \delta\omega/\omega_0 \ll 1$. Using equations (B.1) and (B.2) and neglecting again higher-order terms, we find that

$$v_{\rm f}(t_n) = \frac{q}{m} \int_{-\infty}^{t_n} E(\tau)\, {\rm d}\tau \approx a_1 + n a_2, \tag{B.3}$$

where

$$a_1 = -3q A_1 r \sin\theta / 2m\omega_0, \tag{B.4}$$

$$a_2 = -3q\pi A_1 r \delta\omega \cos\theta / 2m\omega_0^2. \tag{B.5}$$

We further assume that the amplitude $\delta\rho_n$ of each step in the modulation of the plasma density does not depend on the index $n$. For the square-shaped pulse envelope considered here, this

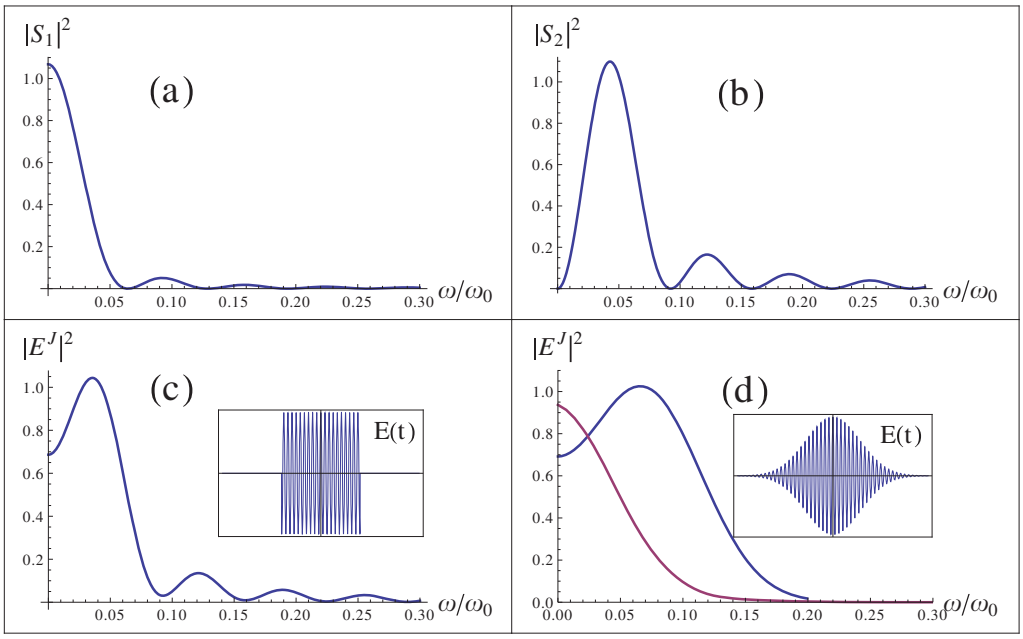


**Figure B.1.** Typical form factors (a) $|S_1|^2$, (b) $|S_2|^2$ and (c) the field $|E^J|^2$ depending on $\tilde{\omega} = \omega/\omega_0$ obtained from equations (B.6), (B.9) and (B.11) for $\theta = \pi/4$, $M = 15$, $r = \sqrt{0.2}$ and $\delta\omega/\omega_0 = 0.0533$ ($\delta\nu = 20$ THz). For comparison, in (d), the spectral shapes from figure 2(c) are repeated (the blue curve corresponds to case 3 ($\nu_0$, $2\nu_0 - \delta\nu$) and the red curve to case 4 ($\nu_0$, $2\nu_0 + \delta\nu$)). The insets in (c) and (d) show the corresponding pump pulse shapes.

essentially means that saturation of the free electron density is neglected. Then, according to equation (4), we have

$$E^J(\omega) \propto (a_1 S_1 + a_2 S_2), \tag{B.6}$$

where

$$S_1 = \sum_n \mathrm{e}^{\mathrm{i}\omega t_n}, \tag{B.7}$$

$$S_2 = \sum_n n\,\mathrm{e}^{\mathrm{i}\,\omega t_n}. \tag{B.8}$$

Here, the summation runs over all ionization events. Following equation (B.2), the exponent $\exp(\mathrm{i}\omega t_n)$ can be expressed as $\exp(-2\mathrm{i}\,r\tilde{\omega}\sin\theta + \mathrm{i}ng_+\tilde{\omega})$ for even $n$ and $\exp(2\mathrm{i}\,r\tilde{\omega}\sin\theta - \mathrm{i}ng_-\tilde{\omega})$ for odd $n$, where $\tilde{\omega} = \omega/\omega_0$ is the normalized frequency and $g_+ = \pi(2r\delta\omega\cos\theta/\omega_0 + 1)$, $g_- = \pi(2r\delta\omega\cos\theta/\omega_0 - 1)$. Considering an odd number of ionization events $N$, being much larger than unity, we calculate the expressions in equation (B.6) by performing the summation from $-M$ to $M$, where $M = (N-1)/2$. The term $S_1$ in equation (B.7) comprises a simple geometric series and gives after separate summation for odd and even $n$:

$$S_1 \approx \mathrm{e}^{2\mathrm{i}r\tilde{\omega}\sin\theta}\frac{\sin(Mg_+\tilde{\omega})}{\sin(g_+\tilde{\omega})} + \mathrm{e}^{-2\mathrm{i}r\tilde{\omega}\sin\theta}\frac{\sin(Mg_-\tilde{\omega})}{\sin(g_-\tilde{\omega})}, \tag{B.9}$$

where $M \gg 1$, so that $M+1 \approx M$. A similar analysis is possible for the term $S_2$ in equation (B.8). As before, one performs the sum for odd and even values of $n$ separately. We are then left with an arithmetico-geometric series (see, e.g., [50]), i.e. for arbitrary $q$ and integers $m_1, m_2$:

$$\sum_{n=m_1}^{m_2} nq^n = \frac{m_1(q-1)+q+q^{m_1+m_2+1}[m_2(q-1)-1]}{q^{m_1}(q-1)^2}. \tag{B.10}$$

After substituting equation (B.10) into (B.8), we find that

$$S_2 = \frac{\mathrm{i}}{2}\left\{\frac{(M+2)\sin[Mg_-\tilde{\omega}]-M\sin[(M+2)g_-\tilde{\omega}]}{\sin^2(g_-\tilde{\omega})}\exp(-2\mathrm{i}r\tilde{\omega}\sin\theta)\right.$$
$$\left.+\frac{(M+1)\sin[(M-1)g_+\tilde{\omega}]-(M-1)\sin[(M+1)g_+\tilde{\omega}]}{\sin^2(g_+\tilde{\omega})}\exp(2\mathrm{i}r\tilde{\omega}\sin\theta)\right\}. \tag{B.11}$$

Important features can be refound from the above expressions. In particular, for $\delta\omega = 0$, we have $a_2 = 0$ and hence $E^J \propto S_1$. In addition, $g_+ = -g_- = \pi$ and thus, by introducing $\delta t = \pi/\omega_0$, we obtain

$$S_1 \approx 2\cos\left(2r\sin\theta\frac{\omega}{\omega_0}\right)\frac{\sin(M\omega\delta t)}{\sin(\omega\delta t)}. \tag{B.12}$$

Equation (5) given at the end of section 2 is obtained from equation (B.12) by assuming $\theta = 0$ and $N \gg 1$; that is, $M = (N-1)/2 \approx N/2$.

For nonzero detuning $\delta\omega$ we can at least qualitatively reproduce the behavior presented in figure 2 (case 3) and in figure 3(a), i.e. the shift of the maxima of the THz spectra from zero frequency (see figure B.1). The frequency shift obtained from equations (B.6), (B.9) and (B.11) is, however, symmetric with respect to the sign of $\delta\omega$, in contrast to the full LC model. The asymmetry reported in the main text (see, e.g., figure 1(d)) disappears with increasing pulse duration and thus is induced by the presence of the Gaussian pulse envelope.

## References


[1] Tonouchi M 2007 Cutting-edge terahertz technology *Nat. Photonics* **1** 97–105

[2] Sakai K (ed) 2005 *Terahertz Optoelectronics* (Berlin: Springer)

[3] Mittleman D 2002 *Sensing with Terahertz Radiation* (Berlin: Springer)

[4] Liu J, Dai J, Chin S L and Zhang X C 2010 Broadband terahertz wave remote sensing using coherent manipulation of fluorescence from asymmetrically ionized gases *Nat. Photonics* **4** 627–31

[5] Cook D J and Hochstrasser R M 2000 Intense terahertz pulses by four-wave rectification in air *Opt. Lett.* **25** 1210–2

[6] Kress M, Löffler T, Eden S, Thomson M and Roskos H G 2004 Terahertz-pulse generation by photoionization of air with laser pulses composed of both fundamental and second-harmonic waves *Opt. Lett.* **29** 1120–2

[7] Bartel T, Gaal P, Reimann K, Woerner M and Elsaesser T 2005 Generation of single-cycle THz transients with high electric-field amplitudes *Opt. Lett.* **30** 2805–7

[8] Kreß M *et al* 2006 Determination of the carrier-envelope phase of few-cycle laser pulses with terahertz-emission spectroscopy *Nat. Phys.* **2** 327–31

[9] Xie X, Dai J and Zhang X-C 2006 Coherent control of THz wave generation in ambient air *Phys. Rev. Lett.* **96** 075005

[10] Thomson M D, Kreß M, Löffler T and Roskos H G 2007 Broadband THz emission from gas plasmas induced by femtosecond optical pulses: from fundamentals to applications *Laser Photon. Rev.* **1** 349–68

[11] Kim K-Y, Glownia J H, Taylor A J and Rodriguez G 2007 Terahertz emission from ultrafast ionizing air in symmetry-broken laser fields *Opt. Express* **15** 4577–84
[12] Reimann K 2007 Table-top sources of ultrashort THz pulses *Rep. Prog. Phys.* **70** 1597–632
[13] Kim K-Y, Taylor A J, Glownia J H and Rodriguez G 2008 Coherent control of terahertz supercontinuum generation in ultrafast laser–gas interactions *Nat. Photonics* **2** 605–9
[14] Reimann K 2008 Terahertz radiation: a table-top source of strong pulses *Nat. Photonics* **2** 596–7
[15] Babushkin I *et al* 2010 Ultrafast spatiotemporal dynamics of terahertz generation by ionizing two-color femtosecond pulses in gases *Phys. Rev. Lett.* **105** 053903
[16] Petersen P B and Tokmakoff A 2010 Source for ultrafast continuum infrared and terahertz radiation *Opt. Lett.* **35** 1962–4
[17] Wang W-M *et al* 2008 Strong terahertz pulse generation by chirped laser pulses in tenuous gases *Opt. Express* **16** 16999–17006
[18] Wu H-C, ter Vehn J M and Sheng Z-M 2008 Phase-sensitive terahertz emission from gas targets irradiated by few-cycle laser pulses *New J. Phys.* **10** 043001
[19] Silaev A A and Vvedenskii N V 2009 Residual-current excitation in plasmas produced by few-cycle laser pulses *Phys. Rev. Lett.* **102** 115005
[20] Peñano J, Sprangle P, Hafizi B, Gordon D and Serafim P 2010 Terahertz generation in plasmas using two-color laser pulses *Phys. Rev.* E **81** 026407
[21] Sheng Z-M, Mima K, Zhang J and Sanuki H 2005 Emission of electromagnetic pulses from laser wakefields through linear mode conversion *Phys. Rev. Lett.* **94** 095003
[22] Bystrov A, Vvedenskii N and Gildenburg V 2005 Generation of terahertz radiation upon the optical breakdown of a gas *JETP Lett.* **82** 753–7
[23] Gildenburg V B and Vvedenskii N V 2007 Optical-to-THz wave conversion via excitation of plasma oscillations in the tunneling-ionization process *Phys. Rev. Lett.* **98** 245002
[24] D'Amico C *et al* 2007 Conical forward THz emission from femtosecond-laser-beam filamentation in air *Phys. Rev. Lett.* **98** 235002
[25] D'Amico C *et al* 2008 Forward THz radiation emission by femtosecond filamentation in gases: theory and experiment *New J. Phys.* **10** 013015
[26] Kostin V A and Vvedenskii N V 2010 Ionization-induced conversion of ultrashort Bessel beam to terahertz pulse *Opt. Lett.* **35** 247–9
[27] Kim K-Y 2009 Generation of coherent terahertz radiation in ultrafast laser–gas interactions *Phys. Plasmas* **16** 056706
[28] Thomson M D, Blank V and Roskos H G 2010 Terahertz white-light pulses from an air plasma photo-induced by incommensurate two-color optical fields *Opt. Express* **18** 23173–82
[29] Babushkin I, Skupin S and Herrmann J 2010 Generation of terahertz radiation from ionizing two-color laser pulses in ar filled metallic hollow waveguides *Opt. Express* **18** 9658–63
[30] Das J and Yamaguchi M 2010 Tunable narrow band THz wave generation from laser induced gas plasma *Opt. Express* **18** 7038–46
[31] Rodriguez G and Dakovski G L 2010 Scaling behavior of ultrafast two-color terahertz generation in plasma gas targets: energy and pressure dependence *Opt. Express* **18** 15130–43
[32] Ahn J, Efimov A, Averitt R and Taylor A 2003 Terahertz waveform synthesis via optical rectification of shaped ultrafast laser pulses *Opt. Express* **11** 2486–96
[33] D'Amico C, Tondusson M, Degert J and Freysz E 2009 Tuning and focusing THz pulses by shaping the pump laser beam profile in a nonlinear crystal *Opt. Express* **17** 592–7
[34] Jefimenko O D 1966 *Electricity and Magnetism: An Introduction to the Theory of Electric and Magnetic Fields* (New York: Appleton-Century-Crofts)
[35] Uiberacker M *et al* 2007 Attosecond real-time observation of electron tunnelling in atoms *Nature* **446** 627–32
[36] Verhoef A J *et al* 2010 Optical detection of tunneling ionization *Phys. Rev. Lett.* **104** 163904
[37] Frolov M V, Manakov N L, Silaev A A and Vvedenskii N V 2010 Analytic description of high-order harmonic generation by atoms in a two-color laser field *Phys. Rev.* A **81** 063407

[38] Yudin G L and Ivanov M Yu 2001 Nonadiabatic tunnel ionization: looking inside a laser cycle *Phys. Rev.* A **64** 013409
[39] Serebryannikov E E, Verhoef A J, Mitrofanov A, Baltuška A and Zheltikov A M 2010 Analytic description of high-order harmonic generation by atoms in a two-color laser field *Phys. Rev.* A **81** 063407
[40] Bergé L, Skupin S, Nuter R, Kasparian J and Wolf J-P 2007 Ultrashort filaments of light in weakly ionized, optically transparent media *Rep. Prog. Phys.* **70** 1633–713
[41] Zhou Z, Zhang D, Zhao Z and Yuan J 2009 Terahertz emission of atoms driven by ultrashort laser pulses *Phys. Rev.* A **79** 063413
[42] Yost D C, Schibli Th R, Ye J, Tate J L, Hostetter J, Gaarde M B and Schafer K J 2009 Vacuum-ultraviolet frequency combs from below-threshold harmonics *Nat. Phys.* **5** 815
[43] Brunel F 1990 Harmonic generation due to plasma effects in a gas undergoing multiphoton ionization in the high-intensity limit *J. Opt. Soc. Am.* B **7** 521–6
[44] Born M and Wolf E 1997 *Principles of Optics: Electromagnetic Theory of Propagation, Interference and Diffraction of Light* 6th edn (Cambridge: Cambridge University Press)
[45] Dai H and Liu J 2011 Phase dependence of the generation of terahertz waves from two-color laser-induced gas plasma *J. Opt.* **13** 055201
[46] Köhler C *et al* 2011 Directionality of THz emission from photoinduced gas plasmas *Opt. Lett.* **36** 3166–8
[47] Balciunas T *et al* 2011 Tunable THz generation with a CEP-stable multicolor OPA *High Intensity Lasers and High Field Phenomena (OSA Techn. Dig.)* (Washington, DC: Optical Society of America) paper HWC3
[48] Kolesik M and Moloney J V 2004 Nonlinear optical pulse propagation simulation: from Maxwell's to unidirectional equations *Phys. Rev.* E **70** 036604
[49] Dalgarno A and Kingston A E 1960 The refractive indices and Verdet constants of the inert gases *Proc. R. Soc.* A **259** 424
[50] Riley K F and Hobson M P 2011 *Foundation Mathematics for the Physical Sciences* (Cambridge: Cambridge University Press)